

Symbol	Description
Q_{ij}^0	Second order moments before PSF convolution. Without explicit λ dependence it refers to the moments integrated over the whole pass-band.
$I^0(\mathbf{x})$	Photon surface brightness or <i>image</i> describing the source light distribution before smearing by the PSF. Without explicit λ dependence it refers to the counts integrated over the whole pass-band.
$S(\mathbf{x}; \lambda)$	Source intensity as a function of position and wavelength.
Q_{ij}^{obs}	Observed second order moments after PSF convolution. Without explicit λ dependence it refers to the moments integrated over the whole pass-band.
$I^{\text{obs}}(\mathbf{x})$	Observed photon surface brightness or <i>image</i> . Without explicit λ dependence it refers to the counts integrated over the whole pass-band.
$P_{ij}(\mathbf{x})$	Second order moments of the PSF. Without explicit λ dependence it refers to the moments integrated over the whole pass-band.
R_{PSF}	Characteristic size of the PSF estimated as the sum of the second order moments: $\sqrt{P_{11} + P_{22}}$
R_{gal}	Characteristic size of the observed galaxy estimated as the sum of the second order moments: $\sqrt{Q_{11}^{\text{obs}} + Q_{22}^{\text{obs}}}$
$T(\lambda)$	Transmission as a function of wavelength λ .
$\tilde{\gamma}$	Estimate of the complex shear vector.
Q_{ij}^{nograd}	Second order unconvolved moments of a galaxy with no colour gradients.
$F(\lambda)$	Photon flux at a given wavelength λ , such that $F = \int F(\lambda)d\lambda = \int \lambda S(\lambda)d\lambda$, where S is the flux density.
\mathbf{e}^{obs}	Observed complex ellipticity.
P_γ	Response of a galaxy ellipticity to a shear γ . P_γ^{nograd} is the response of a galaxy that is assumed to have no colour gradients, while P_γ^{grad} is the true response.
$I_{\text{nograd}}^0(\mathbf{x})$	Image constructed assuming a galaxy has no colour gradients. This quantity is needed to estimate the bias as described in Section 2.1
$I_{\text{nograd}}^{\text{obs}}(\mathbf{x})$	Observed image obtained after applying a shear to $I_{\text{nograd}}^0(\mathbf{x})$ and convolving by the PSF. Without explicit λ dependence it refers to the moments integrated over the whole pass-band.
$I_{\text{grad}}^{\text{obs}}(\mathbf{x})$	Observed image obtained after applying a shear to the true galaxy profile $I^0(\mathbf{x}; \lambda)$ and convolution by the PSF. Without explicit λ dependence it refers to the moments integrated over the whole pass-band.

Table 1. Summary table of quantities defined in this paper.

given choice of λ_{ref} . In this last case one is able to derive the PSF corrected image by knowing both the flux of the galaxy and the PSF profile as a function of wavelength. This is the case studied by Cypriano et al. (2010).

2.1 Measurement

The need to use a weight function when measuring the shapes of the faint galaxies leads to a bias in shear estimates due to colour gradients. This result applies to all moment-based methods, such as KSB (Kaiser et al. 1995) or DEIMOS (Melchior et al. 2011). However, the fact that one cannot recover the unconvolved image $I^0(\mathbf{x})$ from broad-band observations suggests that ‘fitting methods’ will also be prone to provide biased estimators of the shear unless they are able to account for the existence of colour gradients. For in-

stance, one could attempt to model galaxies with a bulge and disk component, each with their own SED. We proceed to quantify this bias for moment-based methods, but note that our approach can be extended to evaluate the bias for fitting techniques as well.

The first step is to define the bias that is induced by a spatially varying SED. The PSF correction described by Equation (13) is perfect for a galaxy that has no colour gradients. If Equation (13) is used to obtain the unconvolved image of a galaxy, one effectively approximates the observed galaxy with a galaxy that has the same SED, but no colour gradients. This galaxy actually has a different profile and thus its response to the shear and to the PSF is different. For this reason, correcting the galaxy using Equation (13) leads to a biased estimate of the shear. To quantify the resulting bias we define the response P_γ as the link between the observed ellipticity \mathbf{e}^{obs} and the shear γ

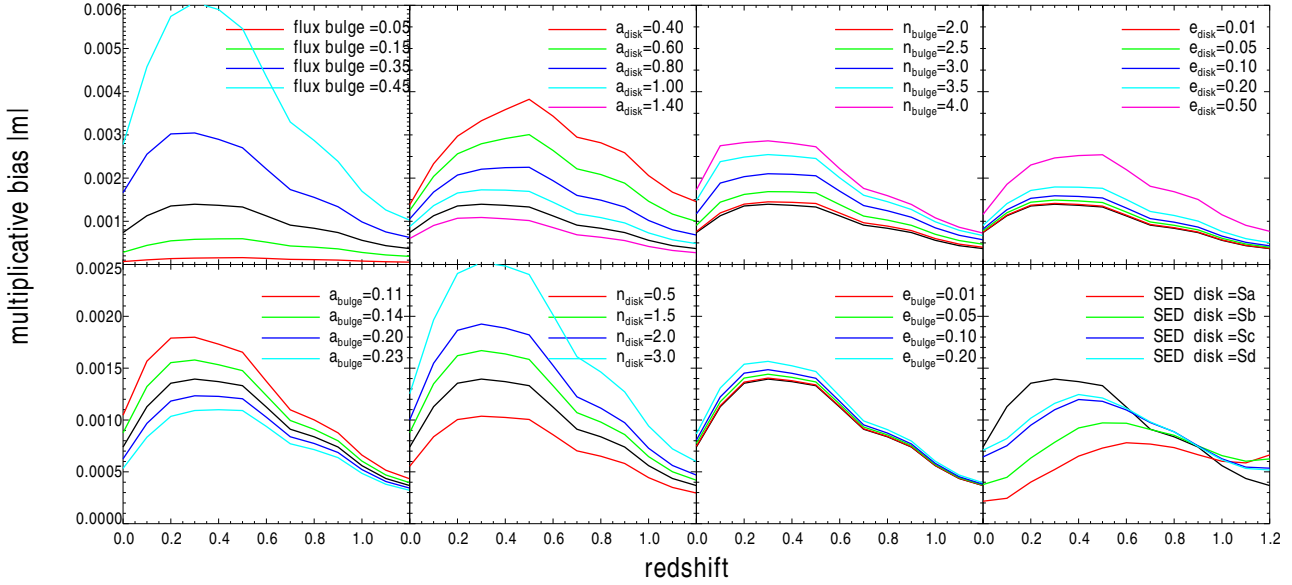


Figure 5. Amplitude of the absolute value of the multiplicative bias for the B galaxy described in Table 3 as a function of redshift, when varying the bulge and disk parameters and using PSF1 (see Table 2). Note that the Sérsic parameters of the disk and bulge are fixed as a function of redshift. For comparison, in each panel the black solid line indicates the bias for the reference galaxy B. Top panels: from left to right we vary the percentage of the light in the bulge, the semi-major axis value of the disk (in arcsec), a_{disk} , the Sérsic index of the bulge, the ellipticity of the disk. In the bottom panels we vary: the characteristic size of the bulge a_{bulge} (in arcsec), the Sérsic index of the disk, the ellipticity of the bulge, the SED of the disk.

which is the case for the majority of galaxies in a typical weak lensing survey.

The blue lines in Figure 3 indicate the noise-to-signal ratio in the measurement of the ellipticity as a function of r_w . Since we are only interested in the relative change, the noise-to-signal ratio is normalised to its value when $r_w = r_h$. Because we ignored the contribution to the noise that depends on the galaxy light profile (see Appendix A of Hoekstra et al. 2000) the ratio is approximately constant for small r_w . Including this term would result in an upturn in the noise-to-signal ratio for small r_w , such that taking $r_w \sim r_h$ minimises the noise-to-signal ratio. Figure 3 shows that the colour-gradient bias decreases rapidly when r_w is increased. The noise-to-signal ratio increases but does so relatively slowly (note the logarithmic scale for the bias and the linear scale for the noise-to-signal ratio). This suggests that adopting $r_w > r_h$ might provide a good compromise between reducing the amplitude of the bias and increasing the noise-to-signal when one needs to account for colour gradients.

4.2 Dependence on the PSF and galaxy characteristics

In this section we study how the bias depends on the PSF characteristics. The bias as a function of redshift for the two reference galaxies B and S is shown in Figure 4. The black solid line indicates the result obtained using the reference PSF (PSF1 in Table 2). The red solid line shows the result for PSF2, which has a larger width resulting in an increase in the bias. More realistic estimates for the actual bias for *Euclid* are obtained using PSF3, indicated by the blue lines in Figure 4; the bias is a factor ~ 2 smaller compared to the results for our reference PSF.

The results presented in Figure 4 are obtained by changing the redshift, but keeping the input Sérsic parameters of the galaxies

fixed. This leads to a change in the observed FWHM because the disk becomes brighter than the bulge as the redshift increases. Since the simulated galaxies have rather extended disks their observed sizes also increases (see the comparison of the FWHM at $z = 0$ and $z = 0.9$ listed in Table 3). Hence, the value of the bias changes with redshift in part because the ratio of the galaxy size to the PSF size changes.

Many parameters contribute to the actual spatial colour variations and it is therefore useful to examine how the bias changes as a function of the bulge and disk characteristics. To do so, we take galaxy B and vary one parameter at a time, keeping all others constant (using PSF1 and adopting $r_w = r_h$). The results are presented in Figure 5. We find that the bias depends most strongly on the flux of the bulge, but also depends on the size of both bulge and disk. It does not depend much on their ellipticity.

In general the bias values range between values of a few times 10^{-4} to a few times 10^{-3} . Note that in all panels the rest-frame colour of the galaxies is the same, except when we vary the fraction of the flux in the bulge (top left panel) or when we change the SED (bottom right panel). These results confirm what we concluded based on Equations (9, 10), i.e. the bias is foremost a function of the colour of the galaxy. Whereas the absolute value of the bias increases when the size of the source galaxy decreases, the changes as a function of the parameters are similar for all galaxies in Table 3. The reference galaxy and its smaller version both have a relatively large disk, which leads to a large FWHM at $z = 0.9$ (see Table 3). Therefore we also consider two galaxies with a smaller FWHM: B4 and S4. The ratio $\text{FWHM}/\text{FWHM}_{\text{PSF}}$ at $z = 0.9$ is 1.3 and 1.1 for B4 and S4, respectively. As one can see from Figure 6, the bias is a very strong function of this ratio: it is smaller than 10^{-3} for a well-resolved galaxy and can become a few percent for a galaxy which is about the size of the PSF.

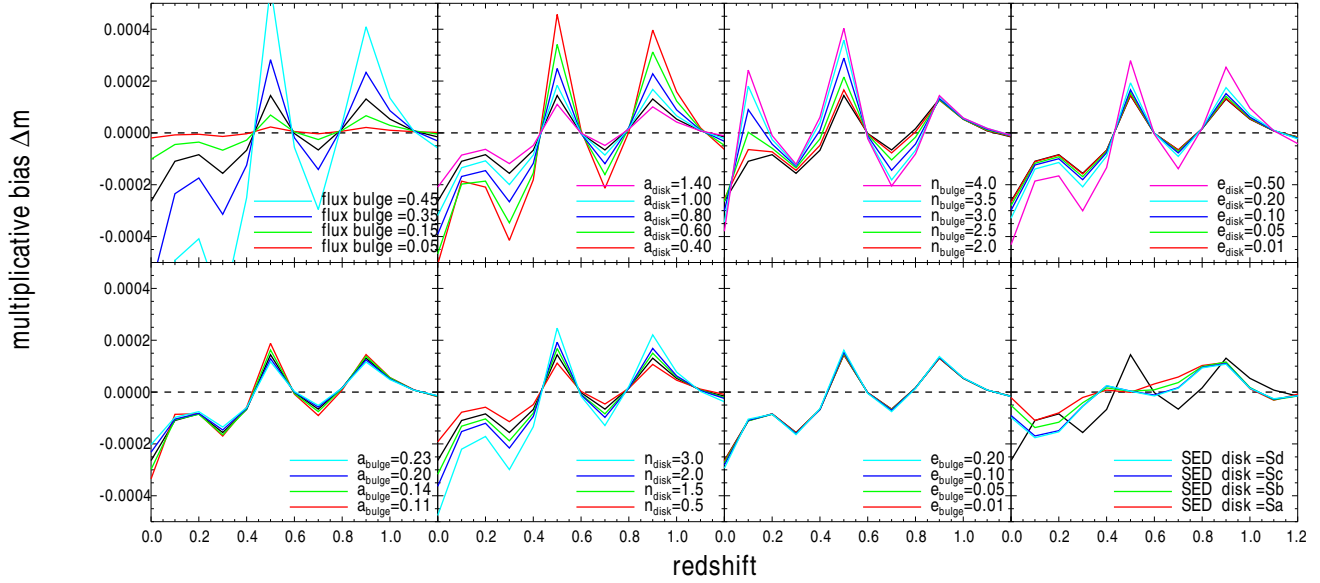


Figure 7. The difference between the predicted bias for an *Euclid*-like broad-band filter and the bias obtained by modelling spatially resolved observations in the *HST* F606W and F814W filters. The results are shown as a function of redshift for model galaxy B, varying the same parameters as was done in Figure 5.

$400 \text{ nm} < \lambda < 600 \text{ nm}$, although this is not the only reason. Not surprisingly, the linear interpolation cannot reproduce any of the SEDs perfectly over the large range in wavelength covered by the *Euclid* pass-band. The linear interpolation fails to capture some of the features of the SEDs visible at $\lambda < 500 \text{ nm}$ and the Balmer break at 400 nm .

Hence the inaccuracy in modelling the SED at each position leads to a residual bias which is a strong function of redshift. However, we note that Figure 7 exacerbates the problem because the local Irr SED is always the same and the linear interpolation fails coherently. In practice, the linear interpolation will sometimes overestimate and sometimes underestimate the bias such that the average bias as a function of redshift might still be estimated correctly and the residuals uncorrelated. The SED also depends on the age of the stellar population, the metallicity, the dust extinction, and the velocity dispersion; all aspects we have neglected. For instance, the bottom-right panel of Figure 7 shows that changing the Irr SED used for the disk to any of the Sa-Sd spectra changes the residual bias substantially.

Finally, it is possible to improve on these results by performing an SED fit instead of a linear interpolation. This might be feasible especially in the case of low redshift galaxies for which multi-colour observations are available and can be used to put tight constraints on the local SED. This could significantly improve the accuracy on the estimated bias at low redshift and help to reduce the residual bias at higher redshifts.

5.2 Effect of the native PSF

Since the images we use to evaluate the colour gradient-induced bias have been convolved with a PSF themselves, the procedure used to retrieve the local SED is more complicated in practice. Accounting for the PSF, Equation (22) changes to

$$\int_{\Delta\lambda_i} \lambda T_i(\lambda) [a(\mathbf{x})\lambda + b(\mathbf{x})] * P_i(\mathbf{x}; \lambda) d\lambda = I_i^{\text{obs}}(\mathbf{x}), \quad i = 1, 2. \quad (25)$$

In Fourier space we obtain a linear system of equations which we can solve to obtain $a(\mathbf{k})$ and $b(\mathbf{k})$, the Fourier transformed maps of the linear coefficients to approximate the local SED. Solving a linear system in Fourier space corresponds to performing a deconvolution. This will therefore cause loss of information, as we cannot reconstruct scales that are smaller than the PSF. Note that this system of equations can be expanded to more filters, and higher order interpolations. The filters might also have different PSFs.

6 EUCLID BIAS MODELLING WITH *HST* FILTERS

In the previous section we have shown that it is possible to quantify the effect of colour gradients using resolved observations in at least two filters. A complication is that one needs to deconvolve the galaxies to account for the native PSF of the narrower filters. This will reduce the overall accuracy of the measurement of the colour gradient bias for two reasons. First of all, solving the system of equations (25) for the local SED is equivalent to a deconvolution, implying that there is an upper limit to the spatial frequencies we can recover. Secondly, the native PSF we need to correct for is not perfectly known.

Since deconvolution algorithms have intrinsic limitations which depend on the size of the PSF, a small PSF is always preferable. Amongst currently available data, *HST* observations are therefore the most suitable to model colour gradients. As can be seen in Figure 8, the characteristic size of the *Euclid* PSF is twice the *HST* PSF. This stems directly from the fact that the diameter of the *Euclid* mirror $D = 1.2 \text{ m}$ is about half of the size of the *HST* mirror, $D = 2.5 \text{ m}$. Despite its small size, there is a loss in accuracy caused by the *HST* PSF. Furthermore, the *HST* PSF does vary as a function

